Journal of Biomolecular NMR, 3 (1993) 133–149
ESCOM

J-Bio NMR 107

^{1}H and ^{15}N resonance assignments and solution secondary structure of oxidized *Desulfovibrio vulgaris* flavodoxin determined by heteronuclear three-dimensional NMR spectroscopy

Brian J. Stockman[a,*], Annica Euvrard[a,**], David A. Kloosterman[a], Terrence A. Scahill[a] and Richard P. Swenson[b]

[a]*Upjohn Laboratories, The Upjohn Company, 301 Henrietta St., Kalamazoo, MI 49007, U.S.A.*
[b]*Department of Biochemistry, Ohio State University, Columbus, OH 43210, U.S.A.*

Received 3 November 1992
Accepted 26 November 1992

Keywords: Structural biology; Isotopic enrichment; Protein–ligand interactions; Cofactor

SUMMARY

Sequence-specific ^{1}H and ^{15}N resonance assignments have been made for all 145 non-prolyl residues and for the flavin cofactor in oxidized *Desulfovibrio vulgaris* flavodoxin. Assignments were obtained by recording and analyzing ^{1}H–^{15}N heteronuclear three-dimensional NMR experiments on uniformly ^{15}N-enriched protein, pH 6.5, at 300 K. Many of the side-chain resonances have also been assigned. Observed medium-and long-range NOEs, in combination with $^{3}J_{NH\alpha}$ coupling constants and $^{1}H^{N}$ exchange data, indicate that the secondary structure consists of a five-stranded parallel β-sheet and four α-helices, with a topology identical to that determined previously by X-ray crystallographic methods. One helix, which is distorted in the X-ray structure, is non-regular in solution as well. Several protein–flavin NOEs, which serve to dock the flavin ligand to its binding site, have also been identified. Based on fast-exchange into $^{2}H_{2}O$, the $^{1}H^{N3}$ proton of the isoalloxazine ring is solvent accessible and not strongly hydrogen-bonded in the flavin binding site, in contrast to what has been observed in several other flavodoxins. The resonance assignments presented here can form the basis for assigning single-site mutant flavodoxins and for correlating structural differences between wild-type and mutant flavodoxins with altered redox potentials.

INTRODUCTION

Flavodoxins are flavin mononucleotide (FMN)-containing proteins that mediate electron transfer at low redox potentials between the prosthetic groups of other proteins (Mayhew and Ludwig, 1975). The flavodoxin from the sulfate-reducing bacteria *Desulfovibrio vulgaris* is a

* To whom correspondence should be addressed.
** Present address: Department of Chemistry, Northwestern University, Evanston, IL 60208-3113, U.S.A.

148-residue protein classified as a short-chain flavodoxin. The flavin cofactor has three oxidation states: oxidized, semiquinone (one-electron reduced), and hydroquinone (two-electron reduced). Protein–flavin mononucleotide interactions shift both the redox potentials of oxidized-semiquinone (E_1) and semiquinone-reduced (E_2) significantly from their free-in-solution values. In *D. vulgaris* flavodoxin, E_1 is −103 mV and E_2 is −438 mV (Dubourdieu et al., 1975), while those of free flavin are −238 mV and −172 mV, respectively (Simondson and Tollin, 1980). An understanding of the specific protein–cofactor interactions that underlie the altered redox potentials is paramount to our understanding of the electron-transfer processes that involve flavodoxins. Structure-function relationships determined for the flavodoxin system should be generally applicable to other electron-transfer proteins.

The structures of flavodoxins from a variety of organisms have been elucidated by both X-ray crystallography (Watenpaugh et al., 1973; Burnett et al., 1974; Smith et al., 1977, 1983; Watt et al., 1991; Fukuyama et al., 1992) and NMR spectroscopy (Stockman et al., 1990; van Mierlo et al., 1990a–c; Clubb et al., 1991). High-resolution X-ray crystallographic structures have been determined for all three redox states of *D. vulgaris* flavodoxin (Watt et al., 1991) and are currently being determined for several single-site variants of this protein (Dr. K.D. Watenpaugh, personal communication). Collectively, these studies have shown that while flavodoxins from a variety of species share a common global fold, the specific protein–flavin interactions vary. These structural differences have proven difficult to correlate with the variations in redox potentials determined for the various flavodoxins (Paulsen et al., 1990).

To identify systematically the specific protein–flavin interactions in *D. vulgaris* flavodoxin that modulate the redox potential, we have begun an investigation to determine the solution structures of the wild-type protein and several single-site variants. Since the redox potentials of the variants are different, the structural changes must account for the differences. As a first step in this process, we have made sequential ^{1}H and ^{15}N resonance assignments for the oxidized wild-type protein. In the process, the solution secondary structure of the protein has been determined, and several protein-FMN interactions have been identified. The resonance assignments for the wild-type protein presented here form the basis for assigning single-site mutant flavodoxins and for correlating structural differences between wild-type and mutant flavodoxins with altered redox potentials.

MATERIALS AND METHODS

Protein enrichment and sample preparation

Recombinant *D. vulgaris* flavodoxin was prepared as described previously (Krey et al., 1988). The protein used for the NMR studies differs from the naturally occurring protein in that the N-terminus methionine has been cleaved off and the proline at the next position has been replaced by an alanine. For comparisons with flavodoxins from other species, the numbering system in this paper begins with the N-terminus alanine as residue number two. Uniformly ^{15}N-enriched flavodoxin was prepared by using M9 minimal media in place of rich media. $^{15}NH_4Cl$ (1 g/l) was supplied as the sole source of nitrogen. Since the flavin cofactor is not supplied in the growth media and must be synthesized from small molecule precursors, the nitrogen atoms of the isoalloxazine ring were also enriched with ^{15}N during this process. After elution from the final ion-exchange column, the protein was dialyzed three times against phosphate buffer. The final sample

for NMR experiments contained 2 mM flavodoxin in 100 mM phosphate buffer at pH 6.5. Trace amounts of PMSF and NaN_3 were added to prevent protease digestion or bacterial growth in the sample. Samples dissolved in ^2H_2O were prepared by lyophilizing the sample and adding 100% ^2H_2O.

NMR spectroscopy

All NMR spectra were recorded at 300 K on a Bruker AMX-600 spectrometer equipped with a multi-channel interface. Proton chemical shifts were referenced to the ^1H_2O signal at 4.76 ppm. Nitrogen chemical shifts were referenced to external $^{15}NH_4Cl$ (2.9 M) in 1 M HCl at 24.93 ppm relative to liquid ammonia. Data were processed on a Silicon Graphics Personal Iris 4D35 workstation, using the software package FELIX from Hare Research, Inc.

Two-dimensional NOESY (Anil Kumar et al., 1980) and DQF-COSY (Piantini et al., 1982) spectra were acquired in ^1H_2O solvent, using standard pulse sequences. Sweep widths of 9 090 Hz were used in both dimensions. In the NOESY experiment, 128 scans were acquired for each of 800 t_1 increments, while in the DQF-COSY experiment, 96 scans were acquired for each of 512 t_1 increments. Quadrature in t_1 was accomplished by using TPPI (Marion and Wüthrich, 1983). Continuous wave low-power saturation was used during the 1.3-s relaxation delay to attenuate the intensity of the ^1H_2O resonance. Since both experiments were recorded on uniformly ^{15}N-enriched protein, a 180° ^{15}N pulse was applied in the center of the evolution period, and GARP decoupling (Shaka et al., 1985) was used during the acquisition period to decouple ^{15}N.

A 2D ^1H–^{15}N HSQC spectrum (Bodenhausen and Ruben, 1980) was acquired in ^1H_2O solvent using ^1H and ^{15}N sweep widths of 9090 Hz and 1953 Hz, respectively. For each of 256 t_1 values, 128 scans were recorded. Quadrature in t_1 was accomplished by using the method of States et al., (1982). Continuous wave low-power saturation was used during the 1.3-s relaxation delay to attenuate the intensity of the ^1H_2O resonance. GARP decoupling (Shaka et al., 1985) was used during acquisition to decouple ^{15}N. Identical spectra were recorded 3 and 24 h after exchanging the protein in ^2H_2O.

A 2D HMQC-J experiment (Kay and Bax, 1990) was recorded in ^1H_2O solvent using the same sweep widths as for the ^1H–^{15}N HSQC spectrum. For each of 1024 t_1 values, 48 scans were recorded. The total measuring time was 22 h. The acquisition time in t_1 was 262 ms, resulting in a digital resolution of 1.9 Hz/pt. During data processing, the t_1 dimension was zero-filled four times for a final spectral resolution of 0.5 Hz/pt. Resolution enhancement in t_1 was accomplished using a combination of Gaussian and Lorentzian multiplications. $^3J_{HN\alpha}$ values, corrected for the linewidth effect (Kay and Bax, 1991), were extracted by measuring the peak-to-peak separation in the 1D ω_1 projection corresponding to the center of each correlation in the 2D spectrum.

Three-dimensional ^1H–^{15}N NOESY-HMQC and TOCSY-HMQC spectra were recorded in ^1H_2O solvent with standard pulse sequences (Marion et al., 1989; Zuiderweg and Fesik, 1989). The ω_2 and ω_3 sweep widths used were the same as for the ^1H–^{15}N HSQC spectrum. The ω_1 sweep width was 7812 Hz, resulting in folding of two of the downfield-shifted ^1H resonances. The reduced ω_1 sweep width improved the resolution in this dimension without adding any resonance overlap. Each 3D experiment was acquired as a series of 2D ^1H–^1H NOESY data sets with incremented ^{15}N evolution periods. Sixteen scans were recorded for each of 256 t_1 values and 32 t_2 values. The total recording time for each experiment was 60 h. Quadrature in t_1 and t_2 was accomplished by using TPPI (Marion and Wüthrich, 1983). ^{15}N was decoupled during t_1 by a

180° pulse in the center of the evolution period, and during t_3 by using a GARP sequence (Shaka et al., 1985). Continuous wave low-power saturation was used during the 1.3-s relaxation delay to attenuate the intensity of the ^1H_2O resonance. A mixing time of 100 ms was used for the NOESY experiment, with low-power saturation of the ^1H_2O resonance during this time period. A DIPSI-2 (Shaka et al., 1988) spin-lock time of 38 ms was used for the TOCSY experiment.

A 3D ^1H–^{15}N HMQC-NOESY-HMQC data set was acquired in ^1H_2O solvent according to Frenkiel et al. (1990). The sweep widths used were identical to those used for the ^1H–^{15}N HSQC spectrum. Thirty-two scans were recorded for each of 64 t_1 and 64 t_2 values. Quadrature in t_1 and t_2 was accomplished by using TPPI (Marion and Wüthrich, 1983). GARP decoupling (Shaka et al., 1985) was used during acquisition to decouple ^{15}N. Continuous wave low-power saturation was used during the 1.3-s relaxation delay to attenuate the intensity of the ^1H_2O resonance. A mixing time of 100 ms was used for the NOESY experiment, with low-power saturation of the ^1H_2O resonance during this time period.

RESULTS AND DISCUSSION

The ready availability of uniformly ^{15}N-enriched flavodoxin allowed us to use a ^{15}N-based sequential assignment strategy (Marion et al., 1989). The 2D ^1H-^{15}N HSQC spectrum of flavodoxin, with the sequence-specific assignments indicated, is shown in Fig. 1. For clarity, the two furthest downfield (^1H) correlations are not shown. The resolution of the $^1H^N$ resonances afforded by the ^{15}N dimension is readily apparent, indicating that 3D spectra should be equally well-resolved and interpretable.

Sequential assignment of the main-chain resonances of oxidized *D. vulgaris* flavodoxin was accomplished for the most part by concerted analysis of two 3D data sets: ^1H–^{15}N NOESY-HMQC and TOCSY-HMQC. All 144 expected $^1H^N$ resonances (147 minus two proline residues and the N-terminus alanine (Krey et al., 1988)) were observed in both spectra, indicating that any saturation transfer arising from presaturation of the water resonance was negligible. In cases of $^1H^N$–$^1H^N$ resonance overlap, $^1H^N$–$^1H^N$ NOEs were assigned using the ^1H–^{15}N HMQC-NOESY-HMQC data set.

The spectra were analyzed in a three-step process. First, symmetry-related pairs of $^1H^N$–$^1H^N$ correlations in the ^1H–^{15}N NOESY-HMQC data set were identified. Since correlations of this type appear twice in the ^1H–^{15}N NOESY-HMQC data set, once at the ^{15}N frequency corresponding to each ^1H–^{15}N unit, they are easy to identify. Identifying these pairs is useful because most of the strong $^1H^N$–$^1H^N$ NOEs arise from sequential residues in either helical or turn conformations. In addition, many of the weaker $^1H^N$–$^1H^N$ NOEs arise from sequential or cross-strand-related residues in regions of β-sheet structure. A $^1H^N$–$^1H^N$ NOE was observed for more than one-half of the residues.

Second, $^1H^N$ resonances were classified into a particular type of spin system, using the ^1H–^{15}N TOCSY-HMQC data set. Excellent magnetization transfer, often extending out to the end of side chains containing methyl groups, facilitated this process for flavodoxin. Alanine and glycine residues, which account for more than 20% of the residues, were particularly easy to identify. Alanine residues were located because of their intense TOCSY correlations to the $^1H^\beta$ methyl group, while glycine residues were identified because of their characteristic ^{15}N chemical shift and two TOCSY correlations to $^1H^\alpha$ resonances. Although not as rigorous, many $^1H^N$ resonances

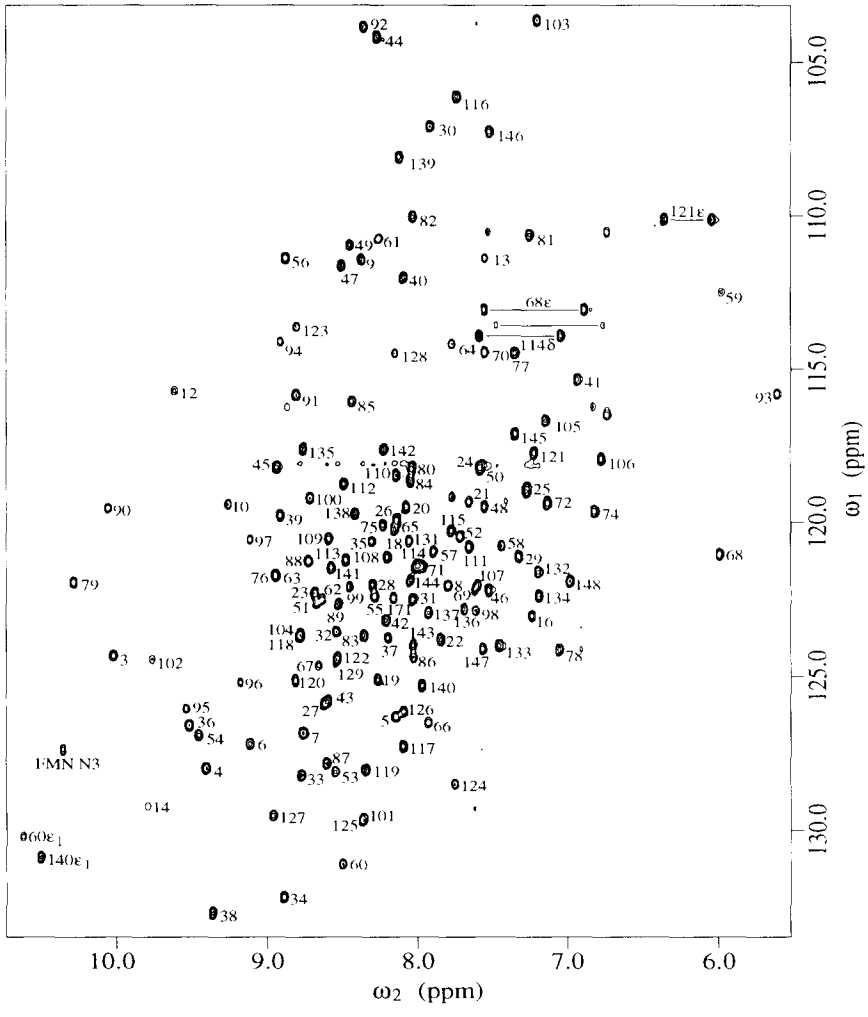

Fig. 1. Region of the 14.2 T ^{1}H–^{15}N HSQC spectrum of uniformly ^{15}N-enriched *D. vulgaris* flavodoxin. Assigned correlations are labeled according to residue sequence number, and, for correlations other than amide backbone nitrogens, atom type. The FMN $^{15}N^{3}$–$^{1}H^{N3}$ correlation is labeled 'FMN N3'. Correlations for the backbone amide groups of threonine[11] and threonine[15] are outside the spectral region shown.

were assigned to three groups: one containing cysteine, aspartic acid, asparagine, and the aromatic amino acids (based on TOCSY correlations to $^{1}H^{\beta}$ resonances between 2.4 and 3.6 ppm), one containing valine, isoleucine, and leucine (based on TOCSY correlations to resonances with methyl-like chemical shifts), and one containing arginine, lysine, glutamine, and glutamic acid (based on TOCSY correlations to $^{1}H^{\beta}$ resonances between 1.6 and 2.4 ppm). The aromatic residues sometimes could be distinguished from the other residues in their category by virtue of a $^{1}H^{N}$–$^{1}H^{\delta}$ NOE in the region of 7.0 ppm.

Finally, residues were aligned sequentially by standard techniques (Wüthrich, 1986). Intraresidue and interresidue correlations in the ^{1}H–^{15}N NOESY-HMQC data set were distinguished by reference to the TOCSY-HMQC data set. Recording the two data sets with identical sweep widths

allowed the corresponding 2D ^1H–^1H slices of each data set to be superimposed on a single sheet of paper, facilitating this process. The excellent dispersion and sharpness of the correlations allowed many stretches of ten or more residues to be aligned. Classification of the $^1H^N$ groups to particular types allowed the stretches to be placed uniquely in the primary sequence of the protein. Three examples will be presented, corresponding to the three regions of the protein that interact with the FMN cofactor. Each is representative of the quality of data obtained.

Residues 5–15 interact with the ribityl and phosphate moieties of the cofactor, forming numerous hydrogen bonds that anchor the FMN group into the protein (Watenpaugh et al., 1973; Watt et al., 1991). The assignments for this stretch of residues are shown in Fig. 2. Each panel represents a small ω_1,ω_3 slice of the ^1H–^{15}N NOESY-HMQC spectrum corresponding to the $^1H^N$ group of the residue indicated. Intraresidue NOEs are boxed. Arrows drawn indicate sequential dNα(i,i−1) and dNβ(i,i−1) NOEs used to make the assignments. Horizontal lines identify sequential dNN NOEs. Sequential dNα(i,i−1) correlations were observed for all residues except glycine[13]. The connection between Thr[12] and Gly[13] was made from the dNN NOE observed between these two residues. From the ^1H–^{15}N TOCSY-HMQC spectrum, side-chain assignments were made for all residues except Thr[12]. Sequential $^1H^N$–$^1H^N$ and dNα(i,i−2) correlations observed for residues 10–13 locate a type I turn at this position. The low-field chemical shifts of the $^1H^N$ resonances of residues 11–15 have been observed in other flavodoxins (Clubb et al., 1991) and probably arise from the hydrogen bonding of these atoms to the phosphate group of FMN.

Residues 57–67 comprise one of two loops of the protein that interact with the isoalloxazine ring portion of FMN. As shown in Fig. 3, unambiguous sequential dNα(i,i−1) and dNβ(i,i−1) correlations were observed for all residues, except aspartic acid[63], in the ^1H–^{15}N NOESY-HMQC data set. However, a weak $^1H^N$–$^1H^N$ NOE was observed between Asp[62] and Asp[63], allowing these residues to be assigned sequentially. Most of the side-chain resonances of residues in this stretch were assigned from the ^1H–^{15}N TOCSY-HMQC data set. Trp[60] is particularly important because its side chain interacts with the FMN. The side-chain $^1H^{\varepsilon 1}$ resonance and several other aromatic resonances have been assigned for this residue based on the observed NOEs.

The second loop of the protein that interacts with FMN is made up of residues 94–103. Assignment of this stretch of residues is shown in Fig. 4. Unambiguous dNα(i,i−1) correlations were identified for each pair of sequential residues in the ^1H–^{15}N NOESY-HMQC data set. Several residues had additional sequential dNβ(i,i−1) and dNN correlations as well. The last panel of Fig. 4 shows the region of the ^1H–^{15}N NOESY-HMQC spectrum containing the $^1H^{N3}$ resonance of FMN. This resonance was easily identified because of its ^{15}N chemical shift (159.3 ppm). Several NOEs are observed along the ω_1 dimension in the FMN $^1H^{N3}$ panel. These through-space correlations are indicative of short proton–proton distances between $^1H^{N3}$ and protons of residues that comprise the flavin binding site. Because of spectral symmetry, NOEs to other $^1H^N$ resonances, indicated by double-arrowhead lines in Fig. 4, have been assigned. NOEs between the $^1H^{N3}$ resonance and the $^1H^N$ resonances of Tyr[100], Cys[102], and Gly[103] are indicated. Based on the X-ray crystallographic structure of the protein (Watt et al., 1991), the other observed correlations have been assigned as the $^1H^{\alpha}$ of Phe[101], both $^1H^{\beta}$s of Tyr[98], and the $^1H^{\beta}$ and $^1H^{\gamma 2}$ of Thr[59]. These correlations are structural constraints that define how this part of the flavin cofactor interacts with the protein. Assigned protein–flavin NOEs can be used to monitor structural changes in the flavin binding site that occur with amino acid substitutions.

For several pairs of residues, the $^1H^N$ resonances were degenerate (or very nearly so), prohibit-

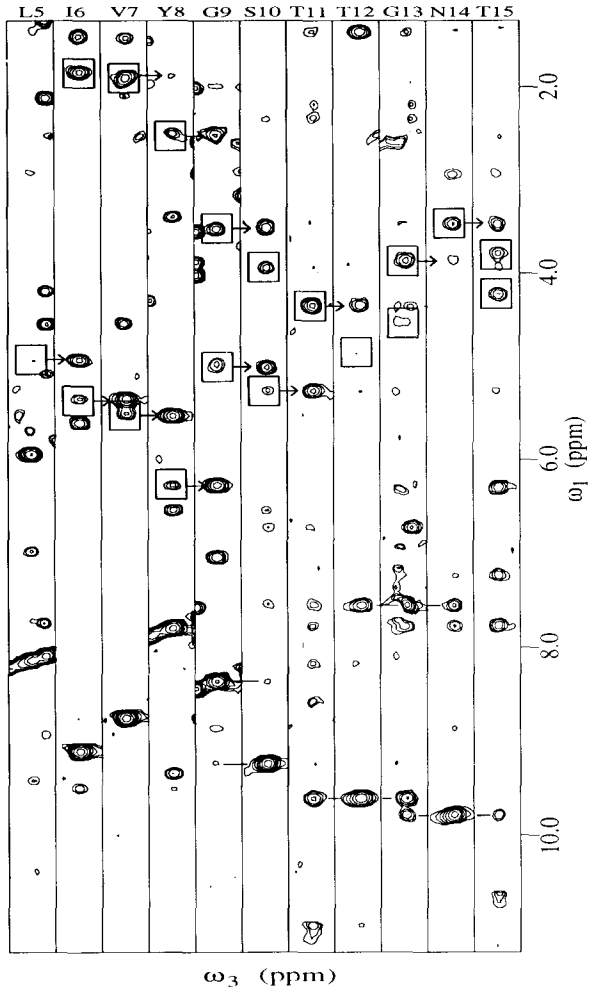

Fig. 2. Selected ω_1,ω_3 slices taken from the 14.2 T 3D ^1H–^{15}N NOESY-HMQC spectrum of flavodoxin. Slices are taken at the ^{15}N frequency (listed in Table 1) corresponding to the residue indicated at the top of each panel. Each slice represents 0.19 ppm in ω_3, with the center located at the frequency of the indicated $^1H^N$ resonance (listed in Table 1). Intraresidue dNα and dNβ correlations are boxed. Sequential dNα(i,i−1) and dNβ(i,i−1) correlations are indicated by arrows beginning at the boxed intraresidue correlation in the preceding slice. Horizontal lines identify sequential dNN NOEs.

ing identification of a $^1H^N$–$^1H^N$ NOE between them. Although this did not prove critical to the assignment process, this information can confirm assignments, and also provides additional information regarding secondary structure. A third 3D spectrum was recorded to identify these NOEs: ^1H–^{15}N HMQC-NOESY-HMQC (Frenkiel et al., 1990). Both the ω_2 and ω_3 dimensions in this spectrum are ^{15}N. $^1H^N$–$^1H^N$ NOEs are located in ω_3 at the $^1H^N$ chemical shift of one residue, and in ω_1 at the ^{15}N chemical shift of the other residue (as opposed to the ^1H chemical shift in the ^1H–^{15}N NOESY-HMQC data set). Provided that the ^{15}N frequencies of the two residues involved in the correlation are not degenerate, the NOE is easily identified. An example of these correla-

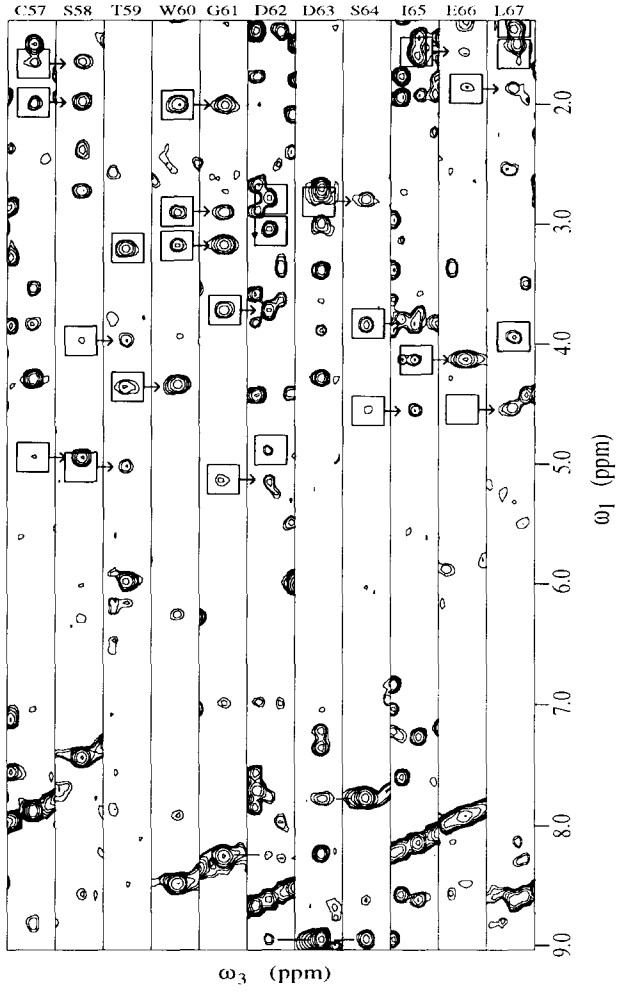

Fig. 3. Selected ω_1,ω_3 slices taken from the 14.2 T 3D ^1H–^{15}N NOESY-HMQC spectrum of flavodoxin. Slices are taken at the ^{15}N frequency (listed in Table 1) corresponding to the residue indicated at the top of each panel. Each slice represents 0.19 ppm in ω_3, with the center located at the frequency of the indicated $^1H^N$ resonance (listed in Table 1). Intraresidue dNα and dNβ correlations are boxed. Sequential dNα(i,i−1) and dNβ(i,i−1) correlations are indicated by arrows beginning at the boxed intraresidue correlation in the preceding slice. Horizontal lines identify sequential dNN NOEs. In the Glu^{66} slice, the weak intraresidue dNα correlation is not seen at this level; however, a strong correlation is seen at the corresponding position in the ^1H–^{15}N TOCSY-HMQC spectrum.

tions for the carboxy terminal residues 132–148 is shown in Fig. 5. Each panel represents a small ω_1,ω_3 slice of the ^1H–^{15}N HMQC-NOESY-HMQC spectrum corresponding to the $^1H^N$ group of the residue indicated. Arrows drawn indicate sequential dNN connectivities. The strong $^1H^N$–$^1H^N$ NOEs observed indicate that this sequence of residues is in an α-helix in the protein (Wüthrich, 1986). For Gly^{146} and Ala^{147}, the $^1H^N$ resonances are nearly degenerate, prohibiting assignment of a $^1H^N$–$^1H^N$ NOE between them in the ^1H–^{15}N NOESY-HMQC spectrum. However, since the ^{15}N resonances are not degenerate, the $^1H^N$–$^1H^N$ NOE is readily observed in Fig. 5. From this data set,

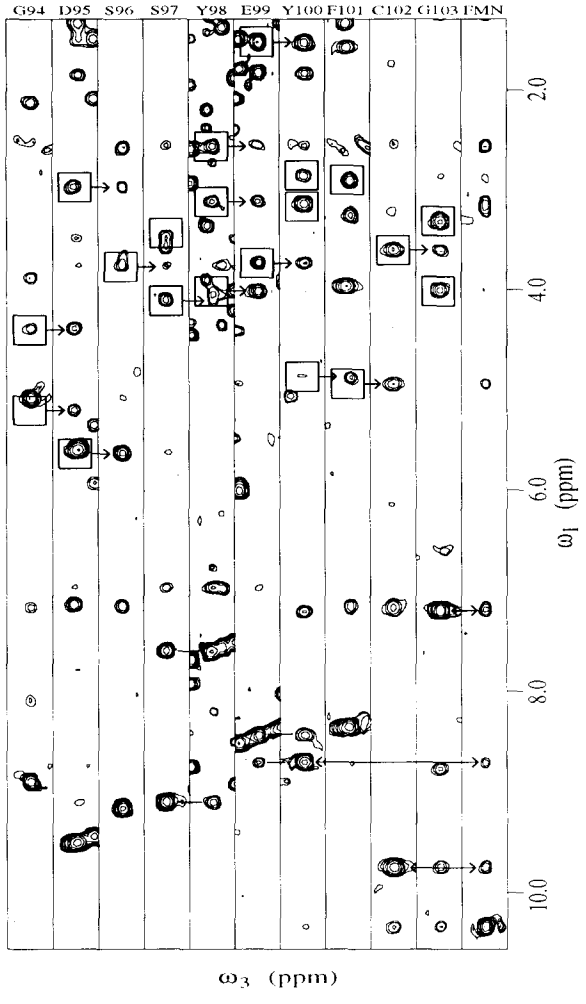

Fig. 4. Selected ω_1,ω_3 slices taken from the 14.2 T 3D ^1H–^{15}N NOESY-HMQC spectrum of flavodoxin. Slices are taken at the ^{15}N frequency (listed in Table 1) corresponding to the residue indicated at the top of each panel. Each slice represents 0.19 ppm in ω_3, with the center located at the frequency of the indicated $^1H^N$ resonance (listed in Table 1). Intraresidue dNα and dNβ correlations are boxed. Sequential dNα(i,i−1) and dNβ(i,i−1) correlations are indicated by arrows beginning at the boxed intraresidue correlation in the preceding slice. Horizontal lines identify sequential dNN NOEs. In the Gly^{94} slice, one weak intraresidue dNα correlation is not seen at this level; however, a strong correlation is seen at the corresponding position in the ^1H–^{15}N TOCSY-HMQC spectrum. Double-arrowhead lines identify NOEs between the FMN $^1H^{N3}$ proton and main-chain $^1H^N$ protons.

four critical $^1H^N$–$^1H^N$ NOEs were identified that could not be extracted from the ^1H–^{15}N NOESY-HMQC data set.

For aliphatic residues and the $^1H^\beta$ resonances of aromatic residues, extension of the main-chain assignments to side-chain assignments was accomplished by comparing the ^1H–^{15}N TOCSY-HMQC and the DQF-COSY spectra. The aromatic protons of the side chains of tyrosine, phenylalanine, and tryptophan were assigned on the basis of NOEs from the $^1H^N$ proton to the

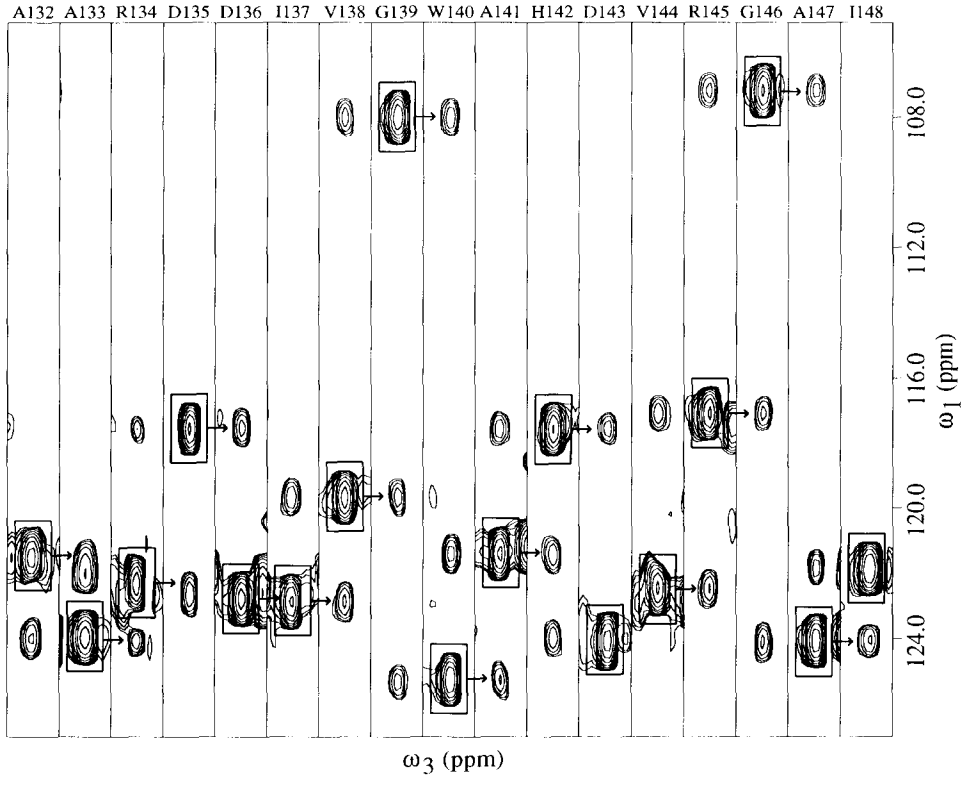

Fig. 5. Selected ω_1,ω_3 slices taken from the 14.2 T 3D ^1H–^{15}N HMQC-NOESY-HMQC spectrum of flavodoxin. Slices are taken at the ^{15}N frequency (listed in Table 1) corresponding to the residue indicated at the top of each panel. Each slice represents 0.19 ppm in ω_3, with the center located at the frequency of the indicated $^1H^N$ resonance (listed in Table 1). The one-bond ^1H–^{15}N correlation for each residue is boxed. Sequential dNN correlations are indicated by arrows beginning at the boxed ^1H–^{15}N correlation in the preceding slice.

side-chain $^1H^\beta$ and $^1H^\delta$ protons in the 3D ^1H–^{15}N NOESY-HMQC spectrum, and from the $^1H^\delta$ protons to the $^1H^\beta$ protons in the 2D NOESY spectrum. Extension from the $^1H^\delta$ to the rest of the ring protons was accomplished by using the DQF-COSY spectrum. The $^1H^{\varepsilon 1}$ protons of both tryptophan residues were easily identified in the ^1H–^{15}N NOESY-HMQC spectrum, as shown in Fig. 1. Tryptophan $^1H^{\varepsilon 1}$ resonances were correlated to the $^1H^\delta$ resonances via $^1H^{\varepsilon 1}$–$^1H^\delta$ correlations in the ^1H–^{15}N TOCSY-HMQC spectrum, and to the rest of the ring protons via NOEs to the $^1H^{\zeta 2}$ resonances in the ^1H–^{15}N NOESY-HMQC spectrum. Glutamine $^1H^\varepsilon$ and asparagine $^1H^\delta$ resonances were assigned by virtue of an NOE to the intraresidue $^1H^\gamma$ or $^1H^\beta$ resonances in the ^1H–^{15}N NOESY-HMQC spectrum.

In total, all main-chain ^1H and ^{15}N resonances were assigned. Partial, and in many case complete, side-chain assignments were made for more than 95% of the residues. A summary of the sequential and medium-range correlations observed is shown in Fig. 6. A list of all assigned resonances is presented in Table I.

NOEs indicative of the solution secondary structure (Wüthrich, 1986) of flavodoxin were identified during analysis of the ^1H–^{15}N NOESY-HMQC data set. These fell into two categories:

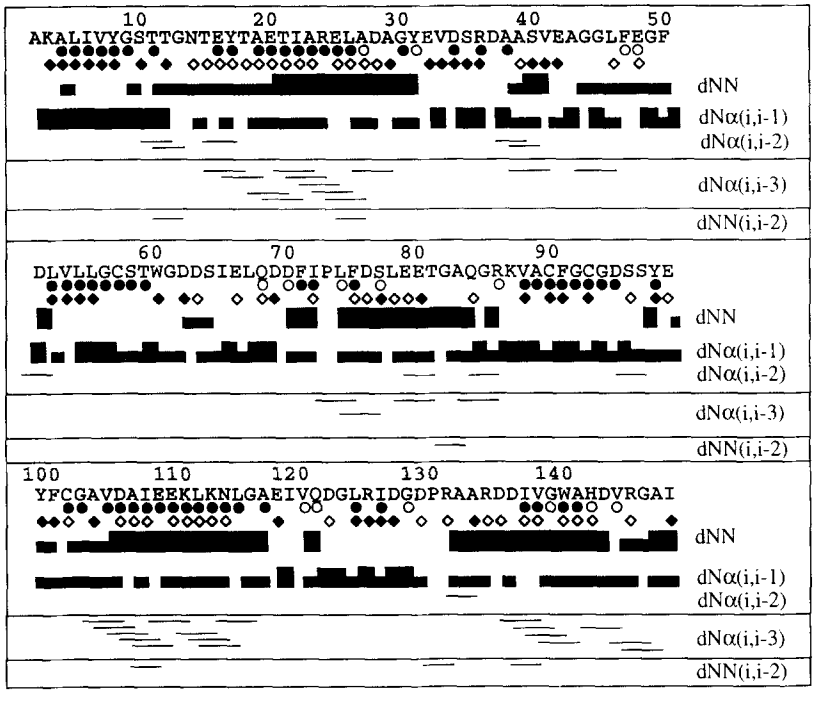

Fig. 6. Summary of sequential resonance assignments of *D. vulgaris* flavodoxin. Circles below a residue indicate that the $^{1}H^{N}$ proton was still detectable after 3 (open) or 24 (filled) h in $^{2}H_{2}O$ solvent. Diamonds below each residue indicate $^{3}J_{HN\alpha}$ values greater than 8 Hz (filled) or less than 6 Hz (open). A bar between two residues indicates that a dNN or dNα(i,i−1) NOE was observed between the two residues. Wide bars indicate a strong intensity NOE, while narrow bars indicate a weak- or medium-intensity NOE. Observed medium-range dNα(i,i−2), dNα(i,i−3), and dNN(i,i−2) NOEs are indicated with horizontal lines between the residues involved.

medium-range NOEs indicative of helical and turn conformations, and long-range NOEs defining the orientation of the β-strands. Figure 6 shows the medium-range NOEs that were identified unambiguously. In some case, resonance degeneracy prohibited assignment of some expected medium-range NOEs, such as several dNα(i,i−3) NOEs in the middle of an α-helix. Additional information about the location of secondary structure was obtained by determining which backbone $^{1}H^{N}$ protons had reduced solvent exchange rates, and by measuring $^{3}J_{NH\alpha}$ coupling constants. These parameters are shown for each residue in Fig. 6. Collectively, these criteria delineate a five-stranded β-sheet, four α-helices, and several turns.

Characteristic patterns of strong dNN NOEs, unambiguous weak dNα(i,i−3) NOEs, $^{3}J_{NH\alpha}$ values smaller than 6 Hz, and reduced $^{1}H^{N}$ exchange rates observed in Fig. 6 identify three α-helices quite well. With these criteria, these α-helices comprise residues 15–27, 103–117, and 132–148. In addition to typical medium-range NOEs, residues in each of these stretches had other characteristics expected of residues in α-helices: weak sequential dNα(i,i−1) correlations, weak $^{1}H^{N}$-$^{1}H^{\alpha}$ TOCSY correlations, and high field $^{1}H^{N}$, $^{1}H^{\alpha}$, and $^{15}N^{\alpha}$ chemical shifts (Wüthrich, 1986; Wishart et al., 1991). A less obvious pattern of similar characteristics is seen for residues 70–80, and locates a fourth α-helix at this position. While strong dNN NOEs are observed for each

TABLE 1
CHEMICAL SHIFTS OF ASSIGNED ^{1}H AND ^{15}N RESONANCES OF *D. vulgaris* FLAVODOXIN[a]

Residue	N^{α}	H^{N}	H^{α}	H^{β}	Others
Ala^{2}			4.00	0.89	
Lys^{3}	124.3	10.02	5.49	1.50,1.78	H^{γ} 2.01
Ala^{4}	128.0	9.41	5.96	1.11	
Leu^{5}	126.3	8.15	4.95	−0.89,0.88	H^{γ} 1.00;H^{δ} 0.42,0.55
Ile^{6}	127.2	9.12	5.35	1.85	$H^{\gamma 1}$ 0.79;$H^{\gamma 2}$1.03
Val^{7}	126.8	8.76	5.56	1.90	H^{γ} 0.66,0.81
Tyr^{8}	122.1	7.80	6.28	2.52	H^{δ} 6.54;H^{ε} 6.99
Gly^{9}	111.5	8.38	3.52,5.01		
Ser^{10}	119.4	9.26	5.26	3.47,3.95	
Thr^{11}	133.1	11.67	4.36	1.42	$H^{\gamma 2}$ 0.90;8.58 OH
Thr^{12}	115.7	9.61	4.85	3.15	
Gly^{13}	111.4	7.56	3.85,4.53		
Asn^{14}	129.2	9.79	3.47	2.56,2.92	
Thr^{15}	129.1	12.01	3.79	4.22	$H^{\gamma 2}$ 1.06
Glu^{16}	123.0	7.24	2.90	1.78,1.95	
Tyr^{17}	122.5	8.17	4.03	3.10,3.20	H^{δ} 6.85;H^{ε}7.15
Thr^{18}	121.4	8.01	3.26	4.30	$H^{\gamma 2}$ 0.80
Ala^{19}	125.1	8.27	3.40	1.21	
Glu^{20}	119.5	8.08	3.81	1.80,1.94	
Thr^{21}	119.3	7.66	3.58	4.02	$H^{\gamma 2}$ 0.96
Ile^{22}	123.8	7.85	3.09	1.40	$H^{\gamma 2}$ 0.60
Ala^{23}	122.3	8.69	3.59	1.39	
Arg^{24}	118.3	7.59	3.98	1.90,1.95	
Glu^{25}	119.0	7.27	3.95	1.91,2.08	
Leu^{26}	120.0	8.14	3.74	1.60	
Ala^{27}	125.9	8.63		1.50	
Asp^{28}	122.0	8.30	4.45	2.62,2.79	
Ala^{29}	121.1	7.32	4.46	1.46	
Gly^{30}	107.2	7.92	3.72,4.31		
Tyr^{31}	121.9	8.05	4.41	2.45,2.55	H^{δ} 6.89,H^{ε} 6.55
Glu^{32}	123.6	8.56	4.55	2.10	
Val^{33}	128.2	8.79	4.92	1.98	H^{γ} 0.85
Asp^{34}	132.2	8.89	4.89	2.66,2.97	
Ser^{35}	120.6	8.30	5.60	3.48,3.76	
Arg^{36}	126.6	9.52	4.63	1.30,1.46	
Asp^{37}	123.7	8.20	3.40	2.50	
Ala^{38}	132.7	9.36	3.59	0.91	
Ala^{39}	119.8	8.92	4.19	1.26	
Ser^{40}	112.0	8.10	4.59	3.91,4.01	
Val^{41}	115.4	6.94	4.59	2.08	
Glu^{42}	123.2	8.21	4.41	1.81,1.98	H^{γ} 2.19
Ala^{43}	125.8	8.60	3.49	1.16	
Gly^{44}	104.2	8.27	3.46,3.62		
Gly^{45}	118.2	8.94	3.78,3.95		
Leu^{46}	122.2	7.53			
Phe^{47}	111.6	8.51	4.84	3.10,3.30	H^{δ} 6.69;H^{ε} 6.95
Glu^{48}	119.5	7.56	4.03	2.03	

TABLE 1 (continued)

Residue	N^{α}	H^{N}	H^{α}	H^{β}	Others
Gly^{49}	111.0	8.45	3.57,3.89		
Phe^{50}	118.3	7.60	4.42	2.78,2.93	H^{δ} 6.95;H^{ε} 7.51
Asp^{51}	122.6	8.67	4.61	2.67,2.89	
Leu^{52}	120.5	7.72	4.84	1.40	
Val^{53}	128.1	8.55		1.46	H^{γ} −0.12,0.41
Leu^{54}	126.9	9.45	5.94	2.10	H^{δ} 1.50
Leu^{55}	122.4	8.29	5.46	1.46,1.99	
Gly^{56}	111.4	8.88	1.50,4.30		
Cys^{57}	121.0	7.90	4.94	1.64,2.00	
Ser^{58}	120.8	7.44	5.02	3.98	
Thr^{59}	112.5	5.98	4.34	3.21	$H^{\gamma 2}$ 1.22;6.15 OH
Trp^{60}	131.1	8.50	2.92	2.01,3.18	$H^{\delta 1}$ 6.25;$H^{\zeta 2}$ 8.18;$H^{\eta 2}$ 7.20;$H^{\varepsilon 1}$ 10.62;$N^{\varepsilon 1}$ 130.2
Gly^{61}	110.8	8.26	3.71,5.16		
Asp^{62}	122.5	8.64	4.89	2.80,3.05	
Asp^{63}	121.8	8.95	2.80		
Ser^{64}	114.2	7.78	4.55	3.82	
Ile^{65}	120.3	8.16	4.15	1.59	$H^{\gamma 2}$ 0.62
Glu^{66}	126.5	7.93	4.54	1.34,1.86	
Leu^{67}	124.6	8.66	3.97	1.39,1.50	
Gln^{68}	121.1	5.99	3.35	1.96	H^{γ} 2.38;H^{ε} 6.75,7.55; N^{ε} 113.1
Asp^{69}	122.2	7.62			
Asp^{70}	114.4	7.56	4.35	2.38,3.18	
Phe^{71}	121.5	7.98	3.85	3.29	H^{δ} 6.49;H^{ε} 6.84
Ile^{72}	119.4	7.14	3.63	1.88	$H^{\gamma 1}$ 1.62;$H^{\gamma 2}$ 0.89
Pro^{73}					
Leu^{74}	119.7	6.83	3.76	1.15	
Phe^{75}	120.1	8.23	3.88	2.98,3.40	H^{δ} 7.23;H^{ε} 7.50
Asp^{76}	121.8	8.95	4.28	2.70,2.79	
Ser^{77}	114.5	7.35	3.48	3.98	
Leu^{78}	124.2	7.06	3.80	1.57	
Glu^{79}	122.0	10.29	3.99	2.04	
Glu^{80}	118.3	8.04	4.50	1.80,2.21	
Thr^{81}	110.7	7.26	4.21	2.46	$H^{\gamma 2}$ 0.99
Gly^{82}	110.1	8.03	3.86,4.22		
Ala^{83}	123.7	8.36	3.97	1.33	
Gln^{84}	118.7	8.05	3.64	2.01	
Gly^{85}	116.1	8.44	3.78,4.12		
Arg^{86}	124.4	8.03	4.35	1.85	H^{γ} 1.46,1.80;H^{δ} 3.11,3.59;H^{ε} 6.76;N^{ε} 84.5
Lys^{87}	127.8	8.60	4.96	2.36	
Val^{88}	121.3	8.73	6.01	1.79	H^{γ} 0.73
Ala^{89}	122.7	8.53	4.94	1.50	
Cys^{90}	119.6	10.05	6.01	2.84	
Phe^{91}	115.9	8.81	5.50	2.25,2.35	H^{δ} 6.74;H^{ε} 7.03;H^{ζ} 6.81
Gly^{92}	103.9	8.36	3.56,3.82		
Cys^{93}	115.8	5.61	5.08	1.39,2.58	

TABLE 1 (continued)

Residue	N^{α}	H^{N}	H^{α}	H^{β}	Others
Gly^{94}	114.1	8.91	4.39,5.20		
Asp^{95}	126.0	9.54	5.62	2.97	
Ser^{96}	125.2	9.18	3.78		
Ser^{97}	120.6	9.11	4.10	3.50	
Tyr^{98}	122.9	7.61	4.03	2.58,3.11	H^{δ} 6.99;H^{ε} 7.09
Glu^{99}	122.1	8.45	3.75	1.51,1.81	
Tyr^{100}	119.2	8.72	4.86	2.84,3.18	H^{δ} 7.22;H^{ε} 6.79
Phe^{101}	129.7	8.36	4.96	2.90,3.25	H^{δ} 7.15;H^{ε} 7.69
Cys^{102}	124.4	9.76	3.60		
Gly^{103}	103.7	7.21	3.32,4.01		
Ala^{104}	123.7	8.79	3.60	0.92	
Val^{105}	116.7	7.15	3.15	1.90	H^{γ} 0.57
Asp^{106}	118.0	6.78	4.19	2.72	
Ala^{107}	122.0	7.61	4.15	1.26	
Ile^{108}	121.1	8.22	3.80	1.78	$H^{\gamma 2}$ 1.02
Glu^{109}	120.5	8.59	3.78	2.23	
Glu^{110}	118.5	8.15	3.98	2.08	
Lys^{111}	120.8	7.66	4.10	1.80	
Leu^{112}	118.8	8.50	3.79	2.10	
Lys^{113}	121.2	8.48	4.04	1.95	
Asn^{114}	121.4	8.01	4.50	2.87,3.02	H^{δ} 7.05,7.60;N^{δ} 114.0
Leu^{115}	120.3	7.78	4.37	1.65,1.78	
Gly^{116}	106.1	7.74	3.87,4.28		
Ala^{117}	127.3	8.10		1.26	
Glu^{118}	123.7	8.79	4.41	1.68,1.85	H^{γ} 2.09
Ile^{119}	128.0	8.35		1.91	$H^{\gamma 2}$ 0.96
Val^{120}	125.1	8.82	4.04	2.10	
Gln^{121}	117.8	7.22	4.41	1.71	H^{ε} 6.05,6.37;N^{ε} 110.1
Asp^{122}	124.3	8.52	4.50		
Gly^{123}	113.6	8.81	3.26,3.95		
Leu^{124}	128.5	7.75	3.97	0.41,−1.35	H^{γ} 0.97
Arg^{125}	129.7	8.38	4.57	1.38,1.59	
Ile^{126}	126.1	8.10	4.19	2.12	$H^{\gamma 2}$ 0.70
Asp^{127}	129.5	8.96	5.06	2.56,2.93	
Gly^{128}	114.5	8.15	3.87,4.03		
Asp^{129}	124.5	8.54		2.65,2.81	
Pro^{130}					
Arg^{131}	120.7	8.06	3.82	1.44,1.62	
Ala^{132}	121.6	7.20	4.38	1.46	
Ala^{133}	124.0	7.46	4.90	1.46	
Arg^{134}	122.4	7.19	4.36		
Asp^{135}	117.6	8.76	4.35	2.60	
Asp^{136}	122.8	7.69	4.45	2.60,2.95	
Ile^{137}	123.0	7.92	3.58	1.95	$H^{\gamma 2}$ 0.66
Val^{138}	119.8	8.42	3.30	2.01	H^{γ} 0.71,0.90
Gly^{139}	108.1	8.13	3.71,3.95		
Trp^{140}	125.3	7.97	4.28	3.38	$H^{\delta 1}$ 7.45;$H^{\zeta 2}$ 7.57;$H^{\eta 2}$ 6.76;$H^{\varepsilon 3}$ 7.00;$H^{\zeta 3}$ 6.54; $H^{\varepsilon 1}$ 10.50;$N^{\varepsilon 1}$ 130.9

TABLE 1 (continued)

Residue	N^{α}	H^{N}	H^{α}	H^{β}	Others
Ala^{141}	121.5	8.58	3.64	1.40	
His^{142}	117.6	8.23	4.02	3.39	
Asp^{143}	124.0	8.03	4.30		
Val^{144}	122.5	8.04	3.19	1.26	H^{γ} −0.22,0.35
Arg^{145}	117.2	7.35	3.81		
Gly^{146}	107.3	7.53	3.78,4.08		
Ala^{147}	124.1	7.57	4.38	1.39	
Ile^{148}	121.9	6.99	4.02	1.94	$H^{\gamma 1}$ 1.25;$H^{\gamma 2}$ 0.85
FMN					H^{N3} 10.36;H^{6} 6.98; N^{3} 159.3

[a] Proton chemical shifts are ± 0.02 ppm. Nitrogen chemical shifts are ± 0.1 ppm.

residue in this particular stretch, many non-degenerate dNα(i,i−3) correlations are not observed. In addition, several $^{1}H^{N}$ protons are in fast-exchange with solvent or have only moderately reduced rates, and several $^{3}J_{HN\alpha}$ values are larger than expected for a helical geometry. These observations are in agreement with the X-ray structure, which shows this region to be a distorted α-helix.

Thirty-four long-range NOEs were observed between main-chain resonances and are indicative of β-sheet structure. They were identified in the ^{1}H–^{15}N NOESY-HMQC spectrum as a third $^{1}H^{\alpha}$ NOE to an amide proton (the others being the intraresidue and preceding residue $^{1}H^{\alpha}$s) or as weak, non-sequential $^{1}H^{N}$–$^{1}H^{N}$ NOEs. Stretches of residues giving rise to these types of NOEs also had other characteristics associated with β-sheet residues: reduced $^{1}H^{N}$ solvent exchange rates, $^{3}J_{NH\alpha}$ values greater than 8 Hz, strong sequential dNα(i,i−1) correlations, strong $^{1}H^{N}$–$^{1}H^{\alpha}$ TOCSY correlations, and low field $^{1}H^{N}$, $^{1}H^{\alpha}$, and $^{15}N^{\alpha}$ chemical shifts. Analysis of the pattern of interstrand NOEs results in alignment of the five parallel β-sheet strands, as shown in Fig. 7. Arrows indicate cross-strand NOEs observed.

Turn conformations, identified by assignment of dNα(i,i−2) and dNN(i,i−2) NOEs as indicated in Fig. 6, are located at residues 10–13, 27–31, 38–41, 61–64, 83–86, 97–101, and 130–133. Observed dNN NOEs indicated that residues 10–13, 28–31, and 38–41 are type I turns, while residues 61–64 and 83–86 are type II turns.

Based on ^{15}N chemical shift comparisons, the $^{1}H^{N3}$ proton has been reported to be only weakly hydrogen-bonded, if at all, in the oxidized protein (Vervoort et al., 1986). We did not observe the flavin $^{1}H^{N3}$ resonance in the first ^{1}H–^{15}N HSQC spectrum recorded in $^{2}H_{2}O$, indicating that this proton is both solvent accessible and not strongly hydrogen-bonded when the cofactor is bound to the protein. This is in contrast to what has been reported for the long-chain flavodoxins from *Anabaena* 7120 (Stockman et al., 1990) and *Anacystis nidulans* (Clubb et al., 1991).

CONCLUSIONS

A ^{15}N-directed strategy was used to facilitate the complete main-chain resonance assignment of the non-prolyl residues of *D. vulgaris* flavodoxin. The medium- and long-range NOEs observed

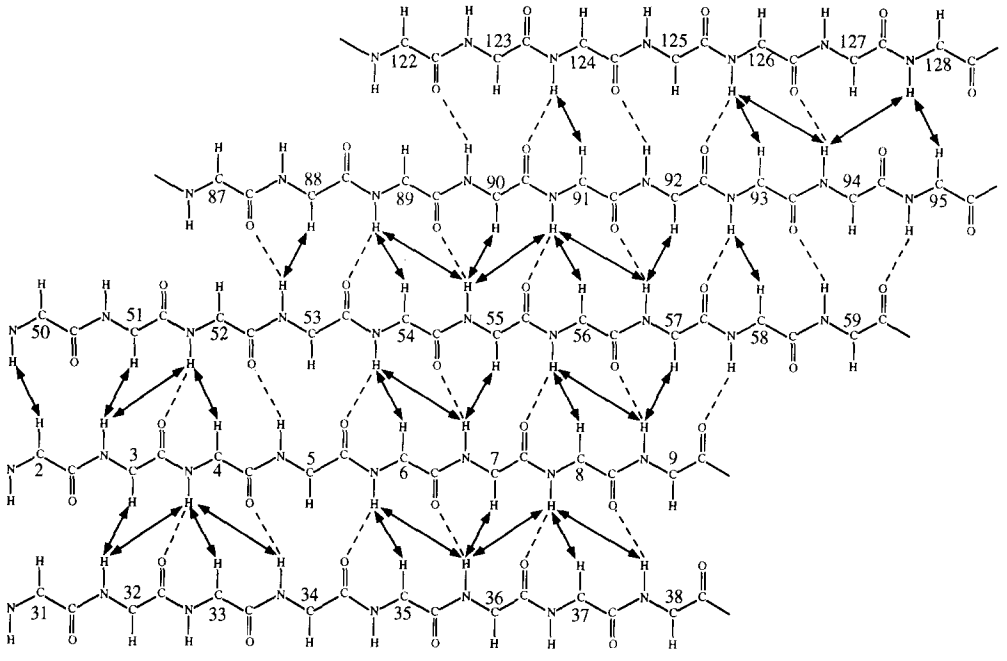

Fig. 7. Schematic diagram of the arrangement of the five-stranded parallel β-sheet framework of *D. vulgaris* flavodoxin. Double-arrowhead lines identify assigned interstrand NOEs. Dashed lines indicate interstrand hydrogen bonds inferred from analysis of $^{1}H^{N}$ exchange rates.

define the solution structure of flavodoxin to be a five-stranded parallel β-sheet surrounded by four α-helices. The secondary structure in solution is identical to that determined previously for the crystalline state (Watenpaugh et al., 1973; Watt et al., 1991). Numerous protein–flavin interactions were identified. These, together with a large number of distance and dihedral angle restraints for the amino acid residues, will allow the solution tertiary structure of the protein to be determined.

The assigned 3D NMR spectra will form a basis for resonance assignments of single-site mutants of the protein. Identified protein–flavin NOEs will be used to monitor structural changes that occur with amino acid substitutions in the flavin binding site, including several substitutions at Tyr^{98} which have already been introduced and partially characterized (Swenson et al., 1991). Structural changes that occur upon mutation of residues in the flavin binding site can then be analyzed in the context of altered redox potentials. The structure–function relationships derived from the solution data will complement that derived from X-ray crystallographic data.

ACKNOWLEDGEMENTS

Supported by NIH Grant GM 36490 to R.P.S. Drs. Keith Watenpaugh and William Watt are appreciated for helpful discussions and their continued collaboration.

REFERENCES

Anil Kumar, Ernst, R.R. and Wüthrich, K. (1980) *Biochem. Biophys. Res. Commun.*, **95**, 1–6.

Bodenhausen, G. and Ruben, D.L. (1980) *Chem. Phys. Lett.*, **69**, 185–188.

Burnett, R.M., Darling, G.D., Kendall, D.S., LeQuesne, M.E., Mayhew, S.G., Smith, W.W. and Ludwig, M.L. (1974) *J. Biol. Chem.*, **249**, 4383–4392.

Clubb, R.T., Thanabal, V., Osborne, C. and Wagner, G. (1991) *Biochemistry*, **30**, 7718–7730.

Dubourdieu, M., Le Gall, J. and Favaudon, V. (1975) *Biochim. Biophys. Acta*, **376**, 519–532.

Frenkiel, T., Bauer, C., Carr, M.D., Birdsall, B. and Feeney, J. (1990) *J. Magn. Reson.*, **90**, 420–425.

Fukuyama, K., Matsubara, H. and Rogers, L.J. (1992) *J. Mol. Biol.*, **225**, 775–789.

Kay, L.E. and Bax, A. (1990) *J. Magn. Reson.*, **86**, 110–126.

Krey, G.D., Vanin, E.F. and Swenson, R.P. (1988) *J. Biol. Chem.*, **263**, 15436–15443.

Marion, D. and Wüthrich, K. (1983) *Biochem. Biophys. Res. Commun.*, **113**, 967–974.

Marion, D., Driscoll, P.C., Kay, L.E., Wingfield, P.T., Bax, A., Gronenborn, A.M. and Clore, G.M. (1989) *Biochemistry*, **28**, 6150–6156.

Mayhew, S.G. and Ludwig, M.L. (1975) *Enzymes*, **12**, 57–118.

Paulsen, K.E., Stankovich, M.T., Stockman, B.J. and Markley, J.L. (1990) *Arch. Biochem. Biophys.*, **280**, 68–73.

Piantini, U., Sørensen, O.W. and Ernst, R.R. (1982) *J. Åm. Chem. Soc.*, **104**, 6800–6801.

Shaka, A.J., Barker, P.B. and Freeman, R. (1985) *J. Magn. Reson.*, **64**, 547–552.

Shaka, A.J., Lee, C.J. and Pines, A. (1988) *J. Magn. Reson.*, **77**, 274–293.

Simondson, R.P. and Tollin, G. (1980) *Mol. Cell. Biochem.*, **33**, 13–24.

Smith, W.W., Burnett, R.M., Darling, G.D. and Ludwig, M.L. (1977) *J. Mol. Biol.*, **117**, 195–225.

Smith, W.W., Pattridge, K.A., Ludwig, M.L., Petsko, G.A., Tsernoglou, D., Tanaka, M. and Yasunobu, K.T. (1983) *J. Mol. Biol.*, **165**, 737–755.

States, D.J., Haberkorn, R.A. and Ruben, D.J. (1982) *J. Magn. Reson.*, **48**, 286–292.

Stockman, B.J., Krezel, A.M., Markley, J.L., Leonhardt, K.G. and Straus, N.A. (1990) *Biochemistry*, **29**, 9600–9609.

Swenson, R.P., Krey, G.D. and Eren, M. (1991) In *Flavins and Flavoproteins* (Eds. Curti, B., Ronchi, S. and Zanetti, G.) Walter de Gruyter, New York, pp. 415–422.

van Mierlo, C.P.M., Lijnzaad, P., Vervoort, J., Muller, F., Berendsen, H.J.C. and de Vlieg, J. (1990a) *Eur. J. Biochem.*, **194**, 185–198.

van Mierlo, C.P.M., van der Sanden, B.P.J., van Woensel, P., Muller, F. and Vervoort, J. (1990b) *Eur. J. Biochem.*, **194**, 199–216.

van Mierlo, C.P.M., Vervoort, J., Muller, F. and Bacher, A. (1990c) *Eur. J. Biochem.*, **187**, 521–541.

Vervoort, J., Müller, F., Mayhew, S.G., van den Berg, W.A.M., Moonen, C.T.W. and Bacher, A. (1986) *Biochemistry*, **25**, 6789–6799.

Watenpaugh, K.D., Sieker, L.C. and Jensen, J.M. (1973) *Proc. Natl. Acad. Sci. USA*, **70**, 3857–3860.

Watt, W., Tulinsky, A., Swenson, R.P. and Watenpaugh, K.D. (1991) *J. Mol. Biol.*, **218**, 195–208.

Wishart, D.S., Sykes, B.D. and Richards, F.M. (1991) *J. Mol. Biol.*, **222**, 311–333.

Wüthrich, K. (1986) *NMR of Proteins and Nucleic Acids*, Wiley, New York.

Zuiderweg, E.R.P. and Fesik, S.W. (1989) *Biochemistry*, **28**, 2387–2391.